

VIP Very Important Paper

Chem
Sus
Chem

Electrochemical Activation of C–C Bonds through Mediated Hydrogen Atom Transfer Reactions

Bing Yan,^[a] Changxia Shi,^[b] Gregg T. Beckham,^[c] Eugene Y.-X. Chen,^[b] and Yuriy Román-Leshkov^{*[a]}

Activating inert sp^3 – sp^3 carbon-carbon (C–C) bonds remains a major bottleneck in the chemical upcycling of recalcitrant polyolefin waste. In this study, redox mediators are used to activate the inert C–C bonds. Specifically, *N*-hydroxyphthalimide (NHPI) is used as the redox mediator, which is oxidized to phthalimide-*N*-oxyl (PINO) radical to initiate hydrogen atom transfer (HAT) reactions with benzylic C–H bonds. The resulting carbon radical is readily captured by molecular oxygen to form a peroxide that decomposes into oxygenated C–C bond-

scission fragments. This indirect approach reduces the oxidation potential by >1.2 V compared to the direct oxidation of the substrate. Studies with model compounds reveal that the selectivity of C–C bond cleavage increases with decreasing C–C bond dissociation energy. With NHPI-mediated oxidation, oligomeric styrene (OS_{510} ; $M_n = 510$ Da) and polystyrene (PS; $M_n \approx 10\,000$ Da) are converted into oxygenated monomers, dimers, and oligomers.

Introduction

The selective activation of sp^3 – sp^3 carbon-carbon (C–C) bonds is a major challenge in organic chemistry, and has recently emerged as a critical step in plastic waste deconstruction and biomass valorization.^[1–7] However, the inertness of the C–C linkages hinders the selective and energy-efficient bond activation in these substrates.^[8–10] Indeed, C–C bond activation is difficult due to several thermodynamic and kinetic constraints,^[11–15] including large bond dissociation energies (BDEs) of around 90 kcal mol^{-1} ,^[11] steric inaccessibility caused by surrounding C–H bonds, and unfavorable orbital directionality towards cleavage which requires the rotation of two carbon sp^3 orbitals.^[16] In some cases, C–C bond scission is facile, for example, for three- or four-membered cycloalkanes with high ring strain, for structures that introduce aromaticity upon cleavage (e.g., the elimination of a methyl group of ergosterol converts the cyclohexadiene ring into a phenyl ring), or for reactants that coordinate strongly to an active site (e.g., pincer-type compounds chelate to the catalyst metal center to direct

the C–C bond cleavage).^[11,16] However, the C–C bonds prevalent in synthetic plastic waste typically do not fall into these special categories and necessitate aggressive reaction conditions for activation.

The thermodynamic and kinetic constraints for C–C bond cleavage have hampered the development of selective plastic depolymerization strategies. For example, thermochemical pathways used for plastic depolymerization, such as pyrolysis and thermal cracking, operate at temperatures $>400^\circ\text{C}$ and suffer from low product selectivity.^[8] Reductive catalytic depolymerization strategies, such as hydrogenolysis and metathesis, improve the energy efficiency by ameliorating reactions conditions (temperatures $>200^\circ\text{C}$), but require reductants such as high-pressure H_2 and/or high-cost noble metal catalysts.^[9,17–21] Oxidative C–C bond cleavage generates oxygenated products as valuable chemicals,^[3] but the traditional thermal catalysis approach requires bromine as a co-catalyst,^[22] impacting on the environment. Photocatalysis shows promising potential in activating inert C–C bonds of plastics to afford oxygenated products, but still suffers from slow reaction rates and low product yields.^[23] These challenges together underscore the need to develop new strategies to depolymerize plastic waste.

To this end, electrochemical oxidation presents a promising approach to activating inert C–C bonds under mild conditions.^[24–29] Such electrochemical approaches may be classified as *direct* or *mediated*. In a direct electrooxidation setup (Figure 1a), the substrate diffuses to the electrode surfaces and undergoes electron transfer. However, the direct electrooxidation is energy ineffective because it requires highly anodic potentials as the driving force to activate the inert C–C bonds,^[30,31] which can also lead to side reactions such as solvent oxidation. On the other hand, in mediated electrooxidation (Figure 1b), a homogeneous, redox-active species is used to mediate the oxidation indirectly by first undergoing reversible oxidation at the electrode, then selectively oxidizing the substrate of interest in solution, and lastly being regenerated at

[a] Dr. B. Yan, Prof. Y. Román-Leshkov
Department of Chemical Engineering
Massachusetts Institute of Technology
Cambridge, Massachusetts 02139 (United States)
E-mail: yroman@mit.edu

[b] Dr. C. Shi, Prof. E. Y.-X. Chen
Department of Chemistry
Colorado State University
Fort Collins, Colorado 80523 (United States)

[c] Dr. G. T. Beckham
Renewable Resources and Enabling Sciences Center and the BOTTLE Consortium
National Renewable Energy Laboratory (NREL)
Golden, Colorado 80402 (United States)

Supporting information for this article is available on the WWW under <https://doi.org/10.1002/cssc.202102317>

This publication is part of a Special Collection highlighting "The Latest Research from our Board Members". Please visit the Special Collection at chemsuschem.org/collections.

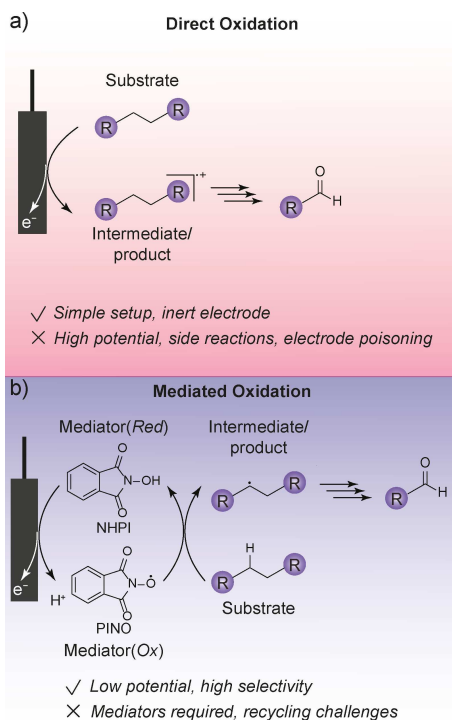


Figure 1. Schematic representation of (a) direct and (b) mediated oxidation to activate C–C bonds. *N*-Hydroxyphthalimide (NHPI) is a mediator active for hydrogen atom transfer (HAT) reactions.

the electrode to start the cycle over. The facile electron transfer of the mediators significantly lowers the oxidation potential. Mediators can also be designed to react with the substrate selectively, thus eliminating many side reactions.

A large number of redox mediators have been explored in electrocatalysis, including organic molecules, transition metal complexes, and inorganic salts, which exhibit a wide range of redox potentials and reactivity.^[30–32] For example, 2,2,6,6-tetramethylpiperidine *N*-oxyl (TEMPO) mediates hydride transfer for alcohol oxidation;^[19] transition metal salts mediate oxygen transfer or electron transfer to oxidize olefins and aromatics;^[32] and Ni- and Co-salen complexes mediate electron transfer for the reductive cyclization of unsaturated aldehydes, ketones, and esters.^[32] Among the redox mediators, *N*-hydroxyphthalimide (NHPI) is well-known to mediate hydrogen atom transfer (HAT). NHPI is readily oxidized at a carbon electrode into the phthalimide-*N*-oxyl (PINO) radical,^[33–37] which is adept at benzylic C–H HAT to return to its reduced form, NHPI, and complete one catalytic cycle (Figure 1b).

In view of the facile electron transfer of NHPI/PINO and the activity of selective benzylic hydrogen atom abstraction, we hypothesize that NHPI/PINO could mediate the activation of inert C–C bonds in polystyrene-type substrates. We demonstrate the NHPI/PINO couple abstracts H from the benzylic C–H bond, making the resulting carbon radical susceptible to further oxidation. The combination of the carbon radical with molecular oxygen forms a peroxide species that decomposes into oxygenated products via spontaneous C–C bond cleavage

events (Figure 1b). We demonstrate the viability of this approach with model compounds including bibenzyl, 1,3-diphenylpropane, 1,4-diphenylbutane, and their derivatives. We also evaluate the mediated oxidation to deconstruct oligomeric styrene ($M_n = 510$ Da, OS_{510}) and polystyrene (PS, ca. 10 000 Da) into oxygenated monomers, dimers, and oligomers as a proof-of-concept of the versatility of this approach towards plastics depolymerization.

Results and Discussion

Cyclic voltammetry confirms that NHPI mediates substrate oxidation

Cyclic voltammetry (CV) was used to study the redox behavior of NHPI. The voltammograms were recorded at 10 mVs^{-1} in 0.1 M $\text{LiBF}_4/\text{acetonitrile}$ electrolyte consisting of 10 mM NHPI. The positions of the oxidative and reductive peak potentials at 1.67 and 0.98 V vs Ag/AgCl, respectively, confirmed the quasi-reversibility of the PINO/NHPI redox couple (Figure S1, black trace). The addition of 0.1 M pyridine shifted the oxidation and reduction potentials negatively to 0.86 and 0.79 V vs Ag/AgCl, respectively (Figure S1, red trace), indicating that the NHPI/PINO redox couple is sensitive to the electrolyte basicity (Figure 1b).

Previous studies have suggested that PINO decomposes in alkaline media.^[33,38] To evaluate the stability of PINO, we gradually dosed acetic acid (HOAc) at 0.02 M increments up to a concentration of 0.10 M. After each dose of HOAc, we recorded a CV scan (Figure S1, blue trace and Figure S2a) and measured the potential separation between the oxidative and reductive peaks (Figure S2b) to assess the reversibility of a redox couple. We note that a reversible reaction exhibits a 57 mV separation between the oxidative and reductive features at room temperature, and this value increases when the reaction becomes increasingly irreversible.^[39] For the NHPI/PINO couple, the oxidative-reductive peak separation decreased from 93.8 to 76.3 mV with increasing HOAc concentration from 0 to 0.10 M, indicating that the redox couple becomes more reversible when the electrolyte turns more acidic. These results suggest that the stability of PINO improves in a HOAc-pyridine buffered electrolyte compared to the pyridine-only electrolyte, in agreement with bulk electrolysis data (see below). Therefore, a HOAc-pyridine buffered electrolyte was used in all experiments unless otherwise stated.

Bibenzyl was used as a model compound to evaluate the catalytic efficacy of PINO. After adding 50 mM bibenzyl to the electrolyte, the PINO reductive feature disappeared and the oxidative current increased compared to that obtained in the absence of bibenzyl (Figure 2, black and red traces), confirming that PINO oxidized bibenzyl. Notably, the potential required to reach a current of 1.0 mA (denoted here as the onset potential) for the NHPI-mediated bibenzyl oxidation was 0.80 V, a value 1.26 V less positive than that for bibenzyl direct oxidation (2.06 V) in the absence of mediators (Figure 2, gray trace). The small anodic feature at approximately 1.5 V in bibenzyl direct

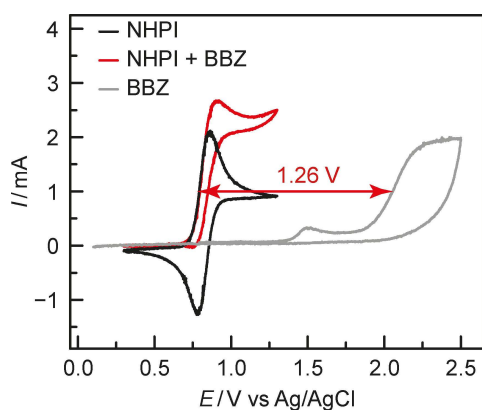


Figure 2. Cyclic voltammetry (CV) plots of 10 mM NHPI/PINO redox couple in the absence (black) and presence of 50 mM bibenzyl (red). The gray trace denotes bibenzyl direct oxidation in the absence of the NHPI mediator. At 1 mA, the NHPI-mediated bibenzyl oxidation requires a potential of 1.26 V less positive than that of direct bibenzyl oxidation. All CVs were recorded at 10 mV s^{-1} in 0.1 M LiBF_4 /acetonitrile electrolyte consisting of 0.1 M pyridine + HOAc.

oxidation is attributed to a pre-activation of the substrate, perhaps leading to the adsorption of bibenzyl to the electrode surfaces.

Bulk electrolysis suggests a bifurcated reaction pathway

We performed bulk electrolysis studies to gain insights into the oxidation reaction pathways. An H-shaped glass cell was used with the working and counter chambers separated by a Nafion membrane (Figure S3). A constant current (typically 2 mA) was applied up to a potential of 1.5 V vs Ag/AgCl, marking the onset of PINO further oxidation. Figure S4 shows a representative chronopotentiometry trace. A steady increase of potential throughout the electrolysis was observed, likely due to an irreversible decomposition of PINO.^[30,40–43] Our analysis of the post-electrolysis electrolyte confirmed the formation of decomposition products of phthalimide and phthalic anhydride (Figures S5 and S6). On average, each molecule of NHPI carries out 7.5 turnovers before undergoing decomposition based on the charge passed during the electrolysis (see the Supporting Information for calculation details).

Products for a typical NHPI-mediated bibenzyl oxidation reaction were identified by gas chromatography-mass spectrometry (GC-MS) and quantified by gas chromatography-flame

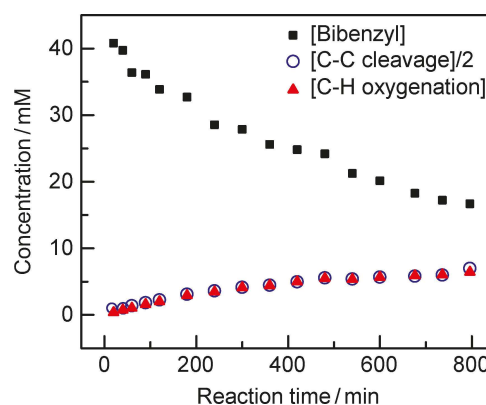


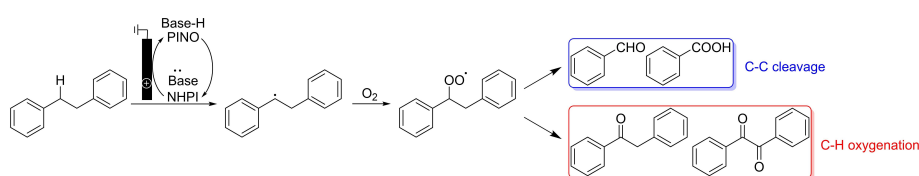
Figure 3. Concentration profiles of bibenzyl, C–C bond cleavage products (benzaldehyde and benzoic acid), and C–H oxygenation products (1,2-diphenylethanone and benzil) during NHPI-mediated bibenzyl oxidation.

ionization detector (GC-FID; Figures S5–S7). Two types of products were observed: (1) C–C bond cleavage products (i.e., benzaldehyde and benzoic acid) and (2) C–H oxygenation products (i.e., 1,2-diphenylethanone and benzil). During the reaction, the electrolyte was sampled and the reaction progress was monitored at regular intervals. The concentration profiles of the C–C bond cleavage products (concentrations were divided by two to account for one molecule of bibenzyl generating two molecules of benzaldehyde or benzoic acid; Figure 3, blue open circle) and C–H bond oxygenation products (Figure 3, red solid triangle) overlap with each other, suggesting that the products originate from a single intermediate that decomposes into either product family with equal probability.

Based on these results, we propose a bifurcated reaction pathway (Scheme 1) wherein: (1) bibenzyl transfers a benzylic C–H to the electrochemically generated PINO; (2) the resulting benzylic carbon radical is captured by O_2 to afford a peroxide radical; and (3) the peroxide radical decomposes in two parallel pathways, one leading to C–C bond cleavage and the other C–H bond oxygenation (Scheme S1).^[22]

Bulk electrolysis condition optimization

We investigated the effects of multiple factors on the oxidation of bibenzyl including NHPI amount, substituents on the NHPI phenyl ring, media basicity, electrolyte types, solvent, O_2 partial pressure, temperature, and oxidation current to explore optimal



Scheme 1. Bifurcated pathway of C–C bond cleavage and C–H oxygenation follows PINO induced HAT and O_2 addition.

conditions for bulk electrolysis. The results are summarized in Table 1 and Tables S1–S5.

Entries 1–4 in Table 1 show the effects of increasing NHPI amount from 2 to 40 mol% with respect to bibenzyl. Higher NHPI concentrations improved bibenzyl conversion, but the Faradaic efficiency (FE%) decreased when NHPI was increased from 10 to 40 mol%. The loss of FE% was mainly due to NHPI/PINO decomposition and pyridine oxidation. We also tested two NHPI derivatives, 3,4,5,6-tetrachloro-*N*-hydroxyphthalimide (Cl_4NHPI) and *N,N'*-dihydroxypyromellitimide (di-NHPI) as alternative redox mediators (Table 1, Entry 5–6). The thermodynamic redox potential of Cl_4NHPI is 0.88 V vs Ag/AgCl (obtained from CV, Figure S8), 60 mV more positive than that of NHPI (0.82 V vs Ag/AgCl, Figure 2), making the PINO radical of Cl_4NHPI more reactive than that of NHPI.^[44] Although higher bibenzyl conversions were observed, Cl_4NHPI generated lower FE% due to higher rates of deleterious side reactions. For di-NHPI, its PINO radical is significantly less stable than PINO.^[42] As a result, the faster decomposition of di-NHPI led to both lower bibenzyl conversion and FE%. We also tested other types of *N*-oxyl radicals including aminoxyls (e.g., TEMPO) and iminoxyls (e.g., oxime radicals; Table S1). However, none of them catalyzed the HAT of bibenzyl. We surmise the lack of reactivity is partly due to a mismatch of BDEs between the C–H bonds of bibenzyl and the NO–H bond of the radical precursors,^[45] and kinetic effects such as the electrophilicity of the *N*-oxyl radical and the transition state configuration of HAT may also play a role.

The effects of electrolyte basicity on NHPI-mediated bibenzyl oxidation were investigated by using varying equimolar mixtures of pyridine and HOAc (Table 1, Entries 3, 8, and 9) or only two equivalents of pyridine (Table 1, Entry 7). The latter featured lower FE% perhaps due to the decomposition of NHPI/PINO. Interestingly, when increasing pyridine and HOAc amounts, both conversion and FE% decreased. These results

suggest that a high concentration of pyridine suppresses the mediated oxidation even in the presence of HOAc.

Using perchloric acid (HClO_4) other than HOAc resulted in drastically reduced conversions and FE% (Table 1, Entries 10 and 11). This is attributed to the positive shift of the NHPI/PINO redox potential with increasing acidity of the electrolyte, which resulted in little bibenzyl conversion at potentials lower than 1.5 V vs Ag/AgCl.

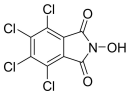
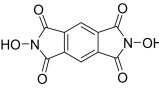
Finally, the effect of basicity was investigated by switching from pyridine to 2,6-lutidine (Table 1, Entry 12) or potassium bicarbonate (KHCO_3 , Table 1, Entry 13). 2,6-Lutidine (conjugate acid $\text{pK}_a=6.72$) is a stronger base than pyridine (conjugate acid $\text{pK}_a=5.25$), resulting in a higher conversion (Entry 12 vs Entry 7). Nevertheless, the methyl groups of 2,6-lutidine are susceptible to PINO HAT as a side reaction, resulting in a lower FE% of bibenzyl oxidation. On the other hand, KHCO_3 generated a lower conversion and FE% compared to pyridine—an effect that is partly due to the poor solubility of KHCO_3 in acetonitrile.

In terms of electrolyte types, we observed that LiClO_4 and TBAPF_6 resulted in a higher bibenzyl conversion but had a much lower FE% compared to LiBF_4 (Table S2). Investigations into electrolyte effects are currently underway.

To gain insight into the role of solvent on bibenzyl oxidation, we carried out reactions in acetonitrile, acetone, and *N,N*-dimethylformamide (DMF) solvents (Table S3). DMF is susceptible to PINO HAT and thus eliminated bibenzyl activity. In acetone, the conversion and FE% were both much lower than those in acetonitrile. The suppressed activity in acetone is likely because acetone facilitates the formation of an NHPI-solvent adduct via hydrogen bonding (e.g., $\text{NO-H}\cdots\text{solvent}$). Since this adduct is less prone to electrochemical oxidation,^[34,40] the activity of bibenzyl oxidation is suppressed.

The effects of O_2 partial pressure were evaluated because O_2 captures the benzylic radical to form the peroxide radical

Table 1. Optimization of preparative bibenzyl oxidation conditions.

Entry	NHPI [mol %] ^[a]	Base [equiv] ^[b]	Electrolyte	Conversion [%] ^[c]	Faradaic efficiency [%]
1	2%	pyridine (Py), HOAc (2, 2)	LiBF_4	16.3	41.3
2	10%	Py, HOAc (2, 2)	LiBF_4	39.5	45.8
3	20%	Py, HOAc (2, 2)	LiBF_4	61.0	45.2
4	40%	Py, HOAc (2, 2)	LiBF_4	82.3	25.6
5	 (Cl_4NHPI) 20%	Py, HOAc (2, 2)	LiBF_4	64.4	38.0
6	 (di-NHPI) 20%	Py, HOAc (2, 2)	LiBF_4	44.0	38.4
7	20%	Py (2)	LiBF_4	61.9	31.5
8	20%	Py, HOAc (4, 4)	LiBF_4	60.2	32.4
9	20%	Py, HOAc (10, 10)	LiBF_4	58.3	26.6
10	20%	Py, HClO_4 (2, 0.4)	LiBF_4	52.1	31.2
11	20%	Py, HClO_4 (2, 1)	LiBF_4	8.2	6.5
12	20%	2,6-Lutidine (2)	LiBF_4	66.5	27.5
13	20%	KHCO_3 (2)	LiBF_4	46.5	18.1

[a] The mole percentage of NHPI is relative to bibenzyl concentration, 50 mM. [b] The equivalent of pyridine and acid is relative to bibenzyl concentration, 50 mM. [c] $\text{Conversion} = \frac{[\text{bibenzyl}]_{\text{initial}} - [\text{bibenzyl}]_{\text{final}}}{[\text{bibenzyl}]_{\text{initial}}} \times 100\%$.

preluding product formation. Specifically, we performed bulk electrolysis in N_2 , 1% O_2 balanced by He, air, and pure O_2 (Table S4). In an N_2 atmosphere, 8.1% of bibenzyl was converted, but no products of C–C bond cleavage or C–H bond oxygenation were detected. This result agrees with the proposed reaction pathway involving a peroxide radical intermediate. With increasing O_2 partial pressure from 0.01 to 1 atm, the conversion improved slightly, but the FE% decreased when 10 or 20 mol% NHPI was used. However, both bibenzyl conversion and FE% increased for 2 mol% NHPI. We attribute the O_2 promotion effects to the improved mass transport of O_2 to the benzylic radical intermediate. The decomposition of NHPI/PINO may explain the decreased FE% at high NHPI concentrations.

The effects of reaction temperature and oxidation current indicate a compromise between reaction rates and NHPI/PINO stability. While a higher temperature or a larger oxidation current can accelerate the reaction, NHPI/PINO decomposition can also be faster. For example, the FE% at 25 °C was higher than the values at 50 and 2 °C, and the conversion at 25 °C was higher than 50 °C but slightly lower than 2 °C (Table S5). The effects of oxidation current are convoluted with the amount of NHPI. At 20 mol% NHPI, the conversion first increased and then decreased with increasing oxidation current from 1 to 5 mA, while the FE% increased with increasing current (Table S6). However, at a lower NHPI (10 mol%), both the conversion and FE% decreased with increasing current (Table S6), suggesting a domination of NHPI self-decomposition. Consequently, both the reaction rate and NHPI/PINO stability should be taken into consideration when optimizing reaction temperature and oxidation current.

Taken together, all these experiments established the optimal NHPI-mediated oxidation conditions to achieve high conversion and FE%: 20 mol% NHPI, 0.1 M pyridine, 0.1 M HOAc, 0.1 M $LiBF_4$ /acetonitrile electrolyte, 1 atm O_2 , room temperature, and an oxidation current of 2 mA. We then applied these reaction conditions to oxidize model compounds and polystyrene samples.

Product selectivity is determined by C–C bond strength

We observed a bifurcated reaction pathway of C–C bond cleavage and C–H bond oxygenation for bibenzyl oxidation (Figure 3, Scheme 1). To investigate the structural factors that affect the product selectivity, several model substrates were evaluated, all containing two phenyl rings but differing in the length of alkyl chains separating the rings and, in the number, and type of substituents on the alkyl chains. These structural variations are expected to alter the C–C bond strength and the reactivity of the C–H bond, and therefore impact product selectivity. Figures S14 and S15 show the representative chronopotentiometry traces of the bulk electrolysis, Table 2 lists the data of conversion, FE%, and selectivity, and Figure 4, Figure S16, and Table S7 show the product distribution for these substrates. The products were characterized by GC–MS, GC–FID, and high-performance liquid chromatography (HPLC).

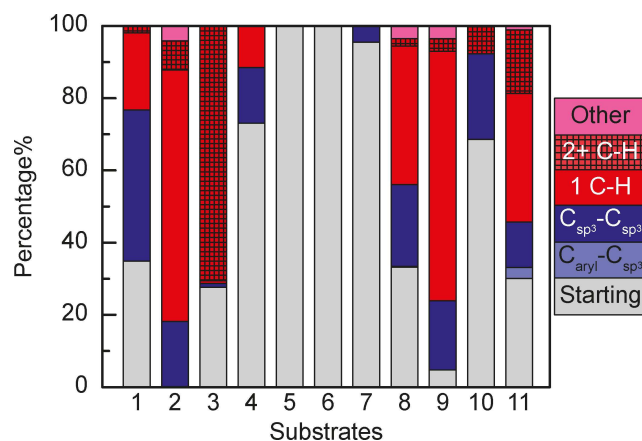
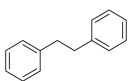
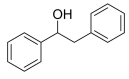
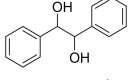
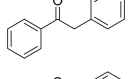
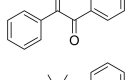
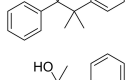
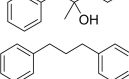
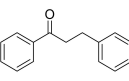
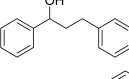
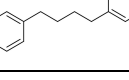
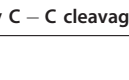


Figure 4. Product distribution of NHPI-mediated oxidation.

We varied the number of sp^3 carbon atoms between the two phenyl rings and evaluated the mediated oxidation of bibenzyl (1), 1,3-diphenylpropane (8; three sp^3 carbon atoms) and 1,4-diphenylbutane (11; four sp^3 carbon atoms). While the conversion of the substrates increased with increasing number of carbon atoms, the selectivity of C–C bond cleavage decreased. In turn, the selectivity of C–H bond oxygenation increased with the number of carbon atoms. Additionally, we detected products from $C_{aryl}-C_{benzyl}$ bond cleavage for (8) (phenol, Figures S16, S17, and S19), and (11) (phenol and benzenebutanal, Figures S16, S20, and S21). Furthermore, products resulting from intramolecular cyclization were also observed for (8) (1,2-diphenylcyclopropane, Figures S16, S18, and S19) and (11) (1,2,3,4-tetrahydro-1-phenylnaphthalene, Figures S16, S20, and S21). We hypothesize that the product distribution is determined by the relative bond strength of C–C and C–H bonds. Table S8 lists the calculated BDEs for these bonds in (1), (8) and (11).^[46,47] Specifically, the weak $C_{benzyl}-C_{benzyl}$ bond of (1) led to its significantly higher selectivity of C–C bond cleavage compared to the other two substrates. The reason why (8) had a higher selectivity of C–C bond cleavage despite its larger C–C BDEs than (11) could be attributed to the stronger C–H bonds of (8) compared to those of (11).

Substituents on the benzylic carbon, namely substrates with one –OH group (1,2-diphenylethanol (2), Table 2, Figures 4, S16, S22–S24) or two –OH groups (*meso*-hydrobenzoin (3), Table 2, Figures 4, S16, S25–S27), also affected the activity of NHPI-mediated oxidation. Since the direct oxidation of *meso*-hydrobenzoin onsets at 1.1 V vs Ag/AgCl (Figure S13a), the bulk electrolysis was terminated when the potential reached 1.1 V (Figure S14b). The conversions for these two substrates were higher than that of (1), while the selectivity to C–C bond cleavage decreased dramatically. After the electrolysis of (2), we detected a product of *N*-(1,2-diphenylethyl)acetamide (Figure S24) that is formed by acetonitrile solvolysis.^[48] It was unclear, however, whether the presence of –OH groups promotes HAT of α C–H bonds, or –OH is oxidized by PINO. Accordingly, we substituted the two benzylic C–H hydrogen atoms in (3) by two methyl groups and performed bulk

Table 2. Results for the NHPI-mediated C–C bond cleavage and C–H bond oxygenation of benzylic substrates.

Entry	Substrate	Conversion [%]	Faradaic efficiency [%]	Selectivity C–C cleavage [%] ^[a]	Selectivity C–H oxygenation [%] ^[b]
1		61.0	45.2	38.4	39.2
2		100	45.8	7.2	61.3
3		80.7	48.6	0.4	61.3
4		26.5	54.3	27.5	43.8
5		14.8	52.4	0.2	0.0
6		4.2	12.5	0.5	1.0
7		11.7	4.5	6.8	0.0
8		71.9	42.0	13.5	47.6
9		96.2	34.1	7.8	59.9
10		41.1	34.9	24.8	15.1
11		76.3	36.6	8.1	56.1

[a] Selectivity C – C cleavage = $\frac{\sum [\text{C–C cleavage products}]}{2([\text{substrate}]_{\text{initial}} - [\text{substrate}]_{\text{final}})} \times 100\%$. [b] Selectivity C – H oxygenation = $\frac{\sum [\text{C–H oxidation products}]}{[\text{substrate}]_{\text{initial}} - [\text{substrate}]_{\text{final}}} \times 100\%$.

electrolysis on the substrate 2,3-diphenyl-2,3-butanediol (**7**) (Table 2, Figures 4, S16, and S28–S30). Similar to (**3**), the direct oxidation of (**7**) onsets at 1.2 V vs Ag/AgCl, and therefore, requires the threshold potential of bulk electrolysis to be set at 1.2 V (Figures S13b and S14f). Notably, minimal products were generated. The results indicate that the alcohol –OH group cannot be oxidized by PINO due to its large BDE (Table S8),^[46,47] which is consistent with previous reports.^[49] Therefore, the presence of –OH groups facilitates the HAT of the α C–H by weakening the α C–H bond (Table S8).^[46,47]

Similarly, methyl or carbonyl groups cannot be oxidized by PINO. For benzil (**5**) (Table 2, Figures 4, S16, S31, and S32) and 2,3-dimethyl-2,3-diphenylbutane (**6**) (Table 2, Figures 4, S16, S33, and S34), no conversion was observed after NHPI-mediated bulk electrolysis. Further, as shown in Table 2 and Figure 4, the carbonyl-containing substrate 1,2-diphenylethanone (**4**) (Figures S16, S35, and S36) led to a much lower conversion and product selectivity. Given that the benzylic C–H BDE of (**4**) (Table S8) is slightly smaller than that of bibenzyl (**1**), we credit the decreased conversion of (**4**) to 1) the reduced number of available benzylic C–H bonds, and 2) a polarity mismatch^[50] between the electron-deficient PINO radical^[51] and the less electron-rich C–H bonds of (**4**) adjacent to the carbonyl group.

Similar substituent studies on the family of 1,3-diphenylpropane were also performed. Compared to (**8**), 1,3-diphenyl-1-propanol (**9**) (Table 2 and Figures 4, S16, S37, and S38) resulted in a significantly higher conversion and dominating product selectivity toward the C–H oxygenation pathway. Analogous to (**2**), we also detected the product formed by acetonitrile solvolysis, *N*-(1,3-diphenylpropyl)acetamide. On the other hand, the substrate 1,3-diphenyl-1-propanone (**10**) (Table 2, Figures 4, S16, S39, and S40) resulted in a lower conversion and a lower selectivity of C–H oxygenation products, while the selectivity of C–C bond cleavage was much higher than that of (**8**). We attribute the improved selectivity to the relatively weak C_{center}–C_{benzyl} bond of (**10**) compared to (**8**) (Table S8).^[46,47] The results of 1,3-diphenylpropane family substrates agree with the conclusions obtained from the bibenzyl family substrates that 1) the –OH group facilitates the benzylic C–H HAT, and 2) the carbonyl group suppresses the PINO oxidation conversion.

Mediated oxidation of oligomeric styrene

We explored the NHPI-mediated oxidation of oligomeric styrene (OS) with a number average molecular weight (M_n) of 510 Da

and a narrow dispersity of 1.05. Details of the oligomers preparation and characterizations can be found in the Supporting Information (Figures S41–S43 for GPC and NMR results).

CV studies confirmed that the oligomeric styrene, denoted as OS₅₁₀, underwent NHPI-mediated oxidation, and the onset potential of the mediated oxidation was 1.01 V less positive than that of the direct oxidation (Figure S44). Notably, there was a small reductive feature in the cathodic sweep, suggesting that the PINO formed in the anodic sweep was not completely consumed by OS₅₁₀. Therefore, in the bulk electrolysis, we applied a constant current of 1 mA instead of 2 mA to slow down the generation of PINO and to suppress NHPI/PINO decomposition. All other standard bulk electrolysis conditions were used. A representative chronopotentiometry is shown in Figure S45. The oxidation progress was monitored by GC-MS (Figure S46–S48) and GC-FID (Figure S49). Here we defined a parameter “unit charge q (F mol^{−1})” to quantify the number of electrons passed per styrene unit: $q = (104 \times Q) / (F \times m)$. Q (C) is the charge passed in electrolysis, F (96485 C mol^{−1}) is the Faradaic constant, m (g) is the weight of OS₅₁₀ added to the electrochemical cell, and 104 (g mol^{−1}) is the molecular weight of one styrene unit. Additional NHPI (10 mM) and pyridine (20 mM) were added once the potential reached 1.5 V vs Ag/AgCl to continue the oxidation.

Figure 5 and Table S9 present the mass yields of oxidation products consisting of zero to five phenyl rings (Ph_{0–5}). Products with more than five phenyl rings were not detectable by GC-FID due to their high boiling points. The yields of Ph_{0–1} products increased with increasing unit charge, from 3.1% ($q=0.57$) to 13.6% ($q=2.28$), indicating the oxidative cleavage of C–C bonds. On the other hand, the yields of longer chain products (Ph_{3–5}) generally decreased with increasing q due to their further oxidation. The simultaneous formation of these products could also lead to an initial rise in the yields at small q values (Ph₃ and Ph₅). The yields of Ph₂ products only oscillated a little across the

oxidation process, suggesting a balance between their formation and further oxidation. The yield of all detected products decreased from 29.4% ($q=0.57$) to 16.7% ($q=2.28$) perhaps because some products were overoxidized, e.g., phenol to ring-opened products.

Based on the product distribution, we propose an oxidation pathway (Scheme S2). Taking a tetramer styrene as an example, the initial step is HAT from a benzylic C–H, affording a benzylic carbon radical. Upon being captured by O₂, a peroxide radical is formed which decomposes into C–C bond scission products. The HAT can take place at either an ending styrene (red branch) or a center one (blue branch), which leads to different products. The products can undergo further mediated oxidation. Besides, the benzylic radical can couple with a PINO radical or form a C=C double bond, leading to minor products other than C–C cleavage or C–H oxygenation.

Polystyrene depolymerization

We employed the NHPI-mediated oxidation strategy to depolymerize polystyrene (PS) as a proof-of-concept. The PS substrate used was an analytical standard for gel permeation chromatography (GPC; 10000 Da) with a low dispersity (1.06). Since PS has a low solubility in acetonitrile, we performed the electrolysis in acetone. For the bulk electrolysis, a constant current of 1 mA was applied (Figure S50 depicts a representative chronopotentiometry trace), same as the oxidation of OS₅₁₀.

The depolymerization progress was monitored by GPC. Additional NHPI (10 mM) and pyridine (20 mM) were added once the potential reached 1.5 V vs Ag/AgCl to continue the depolymerization until all of the starting PS was converted. To measure the molecular weight of the products by GPC, we constructed a calibration curve between the molecular weight of the peak maxima and eluent volume (Figure S43a). The GPC

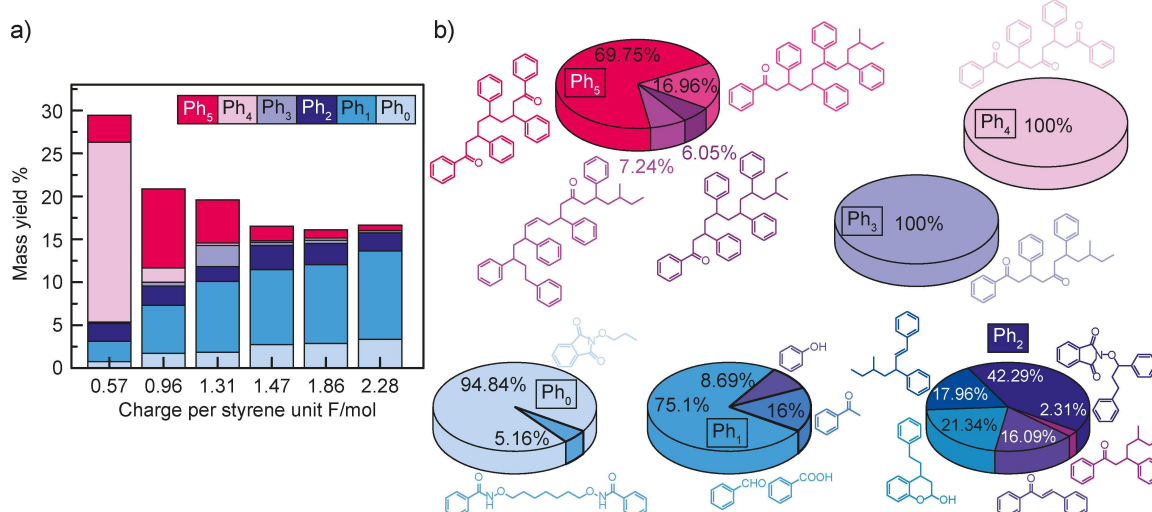


Figure 5. For the mediated oxidation of OS₅₁₀, (a) the mass yields and (b) the distribution of products consisting of zero to five phenyl rings (Ph_{0–5}) depend on the charge passed to each styrene unit in average (unit charge q). Products were quantified by GC-FID. The product distribution was based on the results at $q=2.28$.

results are shown in Figure 6a. Prior to electrolysis, the PS substrate had a peak molecular weight of around 10000 Da. With increasing charge passed, the peak at around 10000 Da decreased and new peaks at lower molecular weight appeared and grew with reaction time. When the unit charge exceeded 1.29 F mol^{-1} , meaning that in average, more than 1.29 electrons were transferred to one styrene unit, all of the starting PS was converted into smaller molecules.

Monomeric (one phenyl ring) and dimeric (two phenyl rings) products of PS depolymerization were identified and quantified by GC-MS (Figure S51) and GC-FID (Figure S52). The results are shown in Figure 6b. At $q=0.44$, the monomer yield was 2.01 % and the dimer yield was 1.91 %. When more current was passed, at $q=4.29$, the monomer yield increased to 7.49 % and the dimer yield to 4.75 %. Three categories of monomers were detected in which the phenyl ring has zero (C_0), one (C_1), or two carbon atoms (C_2) attached to it. Consistent with the small molecule oxidation results, more products with $C_{sp^3}-C_{sp^3}$ bond cleavage (C_1 and C_2 monomers) were observed than phenol ($C_{aryl}-C_{benzyl}$ bond cleavage, C_0). For the dimeric products, three categories of products were identified that differ in the number of carbon atoms between the two phenyl rings: two (C_2), three (C_3), and four carbon atoms (C_4), plus a fourth category of cyclic structures. C_3 molecules were the major dimeric products, in agreement with the repeating unit of PS where the two phenyl rings are separated by three sp^3 carbon atoms.

The ability of NHPI/PINO to activate polystyrene substrates is an encouraging proof of concept that the mediated electrochemical bond activation strategy may be viable to deconstruct polymeric substrates. However, there remain many challenges to achieve effective depolymerization of real PS waste. For example, the slow diffusion and high viscosity of the PS in solution limits the rate of HAT from PS to PINO.^[52–54] Strategies to facilitate mass transfer, such as increasing the operational temperature, using mixed solvents, and vigorous stirring may

improve PS conversion. Besides, a downstream separation approach needs to be developed to purify the wide variety of oxygenate products. For example, advanced separation techniques that employ chromatography or engineered microbes could be used to overcome the heterogeneity of the reaction products.^[55,56] Additionally, PS plastic consists of a number of additives such as metals, metal oxides, pigments, dyes, thermal stabilizers, photo-stabilizers, and other polymers (e.g., acrylonitrile butadiene styrene terpolymer, ABS),^[57–59] which could significantly impact the electrochemical oxidation reactivity. Furthermore, systematic characterization techniques need to be established to identify and quantify the full spectrum of the oxidation products. In particular, the oligomer products cannot be analyzed by GC-FID or GC-MS. We note that the mediated oxidation affords oligomer products spanning the whole range of molecular weights from 300–5000 Da according to GPC, which are challenging to analyze by NMR or LC-MS. Future work is currently underway in our laboratories to address these challenges.

Conclusion

In this study, we developed an electrochemical method to activate inert C–C bonds at room temperature and ambient pressure. We showed that the NHPI/PINO redox couple functions as a mediator that initiates HAT reactions with benzylic C–H. The resulting carbon radical is readily captured by molecular oxygen to afford a peroxide radical that decomposes into oxygenated products. The mediated oxidation approach cleaved C–C bonds of oligomeric styrene ($M_n=510 \text{ Da}$). As a proof-of-concept, we employed NHPI to mediate the oxidative depolymerization of PS (10000 Da) and achieved a yield of monomers and dimers of 12%.

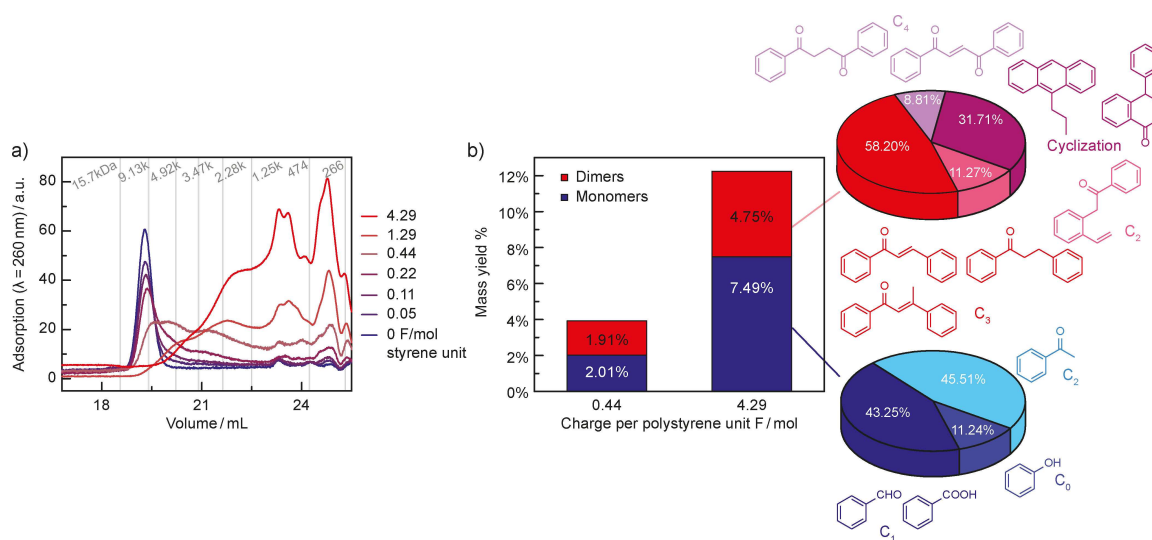


Figure 6. (a) GPC results of NHPI-mediated PS oxidation with increasing unit charge. (b) Monomeric and dimeric product distribution after the bulk electrolysis of PS.

The NHPI-mediated oxidation strategy demonstrates the potential of electrocatalysis in activating inert chemical bonds under mild conditions. Given the wide variety of redox mediators, this study opens the door to employing renewable electricity and targeted redox mediators to catalyze challenging chemical transformations. Future studies will focus on functionalizing the redox mediator to improve its stability in order to boost the conversion and product selectivity. Additionally, strategies to immobilize the redox mediators onto a support or to develop heterogeneous mediators will reduce the self-decomposition of the redox mediators and facilitate the product separation and purification processes, especially for large-scale applications. Furthermore, a flow electrochemical cell with large volumes and electrode surface areas can be developed to scale up the NHPI-mediated oxidation approach in a practical fashion.

Experimental Section

Complete experimental details, GC-MS data, GC-FID data, HPLC data, GPC data, chronopotentiometry results are given in the Supporting Information. This information is available free of charge on the ChemSusChem website at DOI: 10.1002/cssc.202102317.

Acknowledgements

We thank Griffin Drake, Thejas Wesley, Dr. Julie Rorrer, Dr. Ydna Questell-Santiago, and other members of the BOTTLE Consortium for helpful discussions. Funding was provided by the U.S. Department of Energy, Office of Energy Efficiency and Renewable Energy, Advanced Manufacturing Office (AMO) and Bioenergy Technologies Office (BETO). This work was performed as part of the BioOptimized Technologies to keep Thermoplastics out of Landfills and the Environment (BOTTLE) Consortium and was supported by AMO and BETO under Contract DE-AC36-08GO28308 with the National Renewable Energy Laboratory (NREL), operated by Alliance for Sustainable Energy, LLC. The BOTTLE Consortium includes members from MIT and Colorado State University, funded under Contract DE-AC36-08GO28308 with NREL. The views expressed in the article do not necessarily represent the views of the DOE or the U.S. Government. This work was also supported by Eni S.p.A. through the MIT Energy Initiative.

Conflict of Interest

The authors declare no conflict of interest.

Keywords: C–C bond activation • electrocatalysis • plastic upcycling • radical chemistry • redox mediators

[1] C. J. Allpress, L. M. Berreau, *Coord. Chem. Rev.* **2013**, 257, 3005–3029.

[2] W. Wang, M. Wang, X. Li, L. Cai, S. Q. Shi, C. Duan, Y. Ni, *ACS Sustainable Chem. Eng.* **2020**, 8, 38–43.

- [3] J. Zakzeski, P. C. A. Bruijninx, A. L. Jongerius, B. M. Weckhuysen, *Chem. Rev.* **2010**, 110, 3552–3599.
- [4] A. J. Martín, C. Mondelli, S. D. Jaydev, J. Pérez-Ramírez, *Chem* **2021**, 7, 1487–1533.
- [5] A. R. Rahimi, J. M. García, *Nat. Chem. Rev.* **2017**, 1, 1–11.
- [6] I. Vollmer, M. J. F. Jenks, M. C. P. Roelands, R. J. White, T. van Harmelen, P. de Wild, G. P. van der Laan, F. Meirer, J. T. F. Keurentjes, B. M. Weckhuysen, *Angew. Chem.* **2020**, 132, 15524–15548. *Angew. Chem. Int. Ed.* **2020**, 59, 15402–15423.
- [7] L. D. Ellis, N. A. Rorrer, K. P. Sullivan, M. Otto, J. E. McGeehan, Y. Román-Leshkov, N. Wierckx, G. T. Beckham, *Nat. Catal.* **2021**, 4, 539–556.
- [8] D. P. Serrano, J. Aguado, J. M. Escola, *ACS Catal.* **2012**, 2, 1924–1941.
- [9] J. E. Rorrer, G. T. Beckham, Y. Román-Leshkov, *JACS Au* **2021**, 1, 8–12.
- [10] D. M. Wiles, G. Scott, *Polym. Degrad. Stab.* **2006**, 91, 1581–1592.
- [11] C. H. Jun, *Chem. Soc. Rev.* **2004**, 33, 610–618.
- [12] H. Liu, M. Feng, X. Jiang, *Chem.-An Asian J.* **2014**, 9, 3360–3389.
- [13] P. Sivaguru, Z. Wang, G. Zanoni, X. Bi, *Chem. Soc. Rev.* **2019**, 48, 2615–2656.
- [14] T. Kondo, T.-A. Mitsudo, *Chem. Lett.* **2005**, 34, 1462–1467.
- [15] Y. Terao, H. Wakui, T. Satoh, M. Miura, M. Nomura, *J. Am. Chem. Soc.* **2001**, 123, 10407–10408.
- [16] B. Rybtchinski, D. Milstein, *Angew. Chem.* **1999**, 111, 918–932. *Angew. Chem. Int. Ed.* **1999**, 38, 870–883.
- [17] L. D. Ellis, S. V. Orski, G. A. Kenlaw, A. G. Norman, K. L. Beers, Y. Román-Leshkov, G. T. Beckham, *ACS Sustainable Chem. Eng.* **2021**, 9, 623–628.
- [18] F. Zhang, M. Zeng, R. D. Yappert, J. Sun, Y. H. Lee, A. M. LaPointe, B. Peters, M. M. Abu-Omar, S. L. Scott, *Science* **2020**, 370, 437–441.
- [19] G. Celik, R. M. Kennedy, R. A. Hackler, M. Ferrandon, A. Tennakoon, S. Patnaik, A. M. Lapointe, S. C. Ammal, A. Heyden, F. A. Perras, et al., *ACS Cent. Sci.* **2019**, 5, 1795–1803.
- [20] U. Kanbur, G. Zang, A. L. Paterson, P. Chatterjee, R. A. Hackler, M. Delferro, I. I. Slowing, F. A. Perras, P. Sun, A. D. Sadow, *Chem* **2021**, 7, 1347–1362.
- [21] J. E. Rorrer, C. Troyano-Valls, G. T. Beckham, Y. Román-Leshkov, *ACS Sustainable Chem. Eng.* **2021**, 9, 11661–11666.
- [22] W. Partenheimer, *Catal. Today* **2003**, 81, 117–135.
- [23] X. Zhao, B. Boruah, K. Foo Chin, M. Đokić, J. M. Modak, H. Sen Soo, X. Zhao, B. Boruah, K. F. Chin, M. Đokić, et al., *Adv. Mater.* **2021**, 2100843.
- [24] Y. Adeli, K. Huang, Y. Liang, Y. Jiang, J. Liu, S. Song, C. C. Zeng, N. Jiao, *ACS Catal.* **2019**, 9, 2063–2067.
- [25] F. N. Khan, R. Jayakuma, C. N. Pillai, *J. Mol. Catal. A* **2003**, 195, 139–145.
- [26] M. Rafiee, M. Alherech, S. D. Karlen, S. S. Stahl, *J. Am. Chem. Soc.* **2019**, 141, 15266–15276.
- [27] D. Zollinger, U. Griesbach, H. Pütter, C. Comninellis, *Electrochem. Commun.* **2004**, 6, 605–608.
- [28] Y. Kawamata, M. Yan, Z. Liu, D. H. Bao, J. Chen, J. T. Starr, P. S. Baran, *J. Am. Chem. Soc.* **2017**, 139, 7448–7451.
- [29] S. H. Shi, Y. Liang, N. Jiao, *Chem. Rev.* **2021**, 121, 485–505.
- [30] J. E. Nutting, M. Rafiee, S. S. Stahl, *Chem. Rev.* **2018**, 118, 4834–4885.
- [31] F. Wang, S. S. Stahl, *Acc. Chem. Res.* **2020**, 53, 561–574.
- [32] R. Francke, R. D. Little, *Chem. Soc. Rev.* **2014**, 43, 2492–2521.
- [33] M. Rafiee, F. Wang, D. P. Hruszkewycz, S. S. Stahl, *J. Am. Chem. Soc.* **2018**, 140, 22–25.
- [34] S. Coseri, *Catal. Rev.* **2009**, 51, 218–292.
- [35] G. Yang, Y. Ma, J. Xu, *J. Am. Chem. Soc.* **2004**, 126, 10542–10543.
- [36] H. Tateno, Y. Miseki, K. Sayama, *Chem. Commun.* **2019**, 55, 9339–9342.
- [37] A. Barbieri, O. Lanzalunga, A. Lapi, S. Di Stefano, *J. Org. Chem.* **2019**, 84, 13549–13556.
- [38] M. Rafiee, B. Karimi, S. Alizadeh, *ChemElectroChem* **2014**, 1, 455–462.
- [39] J. M. Savéant, *Elements of Molecular and Biomolecular Electrochemistry: An Electrochemical Approach to Electron Transfer Chemistry*, John Wiley and Sons, Hoboken, NJ, USA, **2006**, pp 5–10.
- [40] R. Amorati, M. Lucarini, V. Mugnaini, G. F. Pedulli, F. Minisci, F. Recupero, F. Fontana, P. Astolfi, L. Greci, *J. Org. Chem.* **2003**, 68, 1747–1754.
- [41] N. Koshino, Y. Cai, J. H. Espenson, *J. Phys. Chem. A* **2003**, 107, 4262–4267.
- [42] O. Kushch, O. Kushch, I. Hordieieva, K. Novikova, Y. Litvinov, M. Kompanets, M. Kompanets, A. Shendrik, I. Opeida, I. Opeida, *J. Org. Chem.* **2020**, 85, 7112–7124.
- [43] C. Yang, L. A. Farmer, D. A. Pratt, S. Maldonado, C. R. J. Stephenson, *J. Am. Chem. Soc.* **2021**, 143, 10324–10332.
- [44] E. J. Horn, B. R. Rosen, Y. Chen, J. Tang, K. Chen, M. D. Eastgate, P. S. Baran, *Nature* **2016**, 533, 77–81.
- [45] I. B. Krylov, S. A. Paveliev, A. S. Budnikov, A. O. Terent'ev, *Beilstein J. Org. Chem.* **2020**, 16, 1234–1276.

- [46] P. C. St. John, Y. Guan, Y. Kim, S. Kim, R. S. Paton, *Nat. Commun.* **2020**, *11*, 1–12.
- [47] P. C. St. John, Y. Guan, Y. Kim, B. D. Etz, S. Kim, R. S. Paton, *Sci. Data* **2020**, *7*, 1–6.
- [48] D. M. Camaioni, J. A. Franz, *J. Org. Chem.* **1984**, *49*, 1607–1613.
- [49] F. D'Acunzo, P. Baiocco, M. Fabbri, C. Galli, P. Gentili, *New J. Chem.* **2002**, *26*, 1791–1794.
- [50] C. Le, Y. Liang, R. W. Evans, X. Li, D. W. C. MacMillan, *Nature* **2017**, *547*, 79–83.
- [51] I. B. Krylov, A. S. Budnikov, E. R. Lopat'Eva, O. O. Segida, S. A. Paveliev, A. O. Terent'Ev, *J. Phys. Conf. Ser.* **2021**, *1942*, 012007.
- [52] S. U. Li, J. L. Gainer, *Ind. Eng. Chem. Fundam.* **1968**, *7*, 433–440.
- [53] O. Urakawa, S. F. Swallen, M. D. Ediger, E. D. Von Meerwall, *Macromolecules* **2004**, *37*, 1558–1564.
- [54] J. Rauch, W. Köhler, *J. Chem. Phys.* **2003**, *119*, 11977–11988.
- [55] J. G. Linger, D. R. Vardon, M. T. Guarnieri, E. M. Karp, G. B. Hunsinger, M. A. Franden, C. W. Johnson, G. Chupka, T. J. Strathmann, P. T. Pienkos, et al., *Proc. Natl. Acad. Sci. USA* **2014**, *111*, 12013–12018.
- [56] S. Y. Lee, H. U. Kim, T. U. Chae, J. S. Cho, J. W. Kim, J. H. Shin, D. I. Kim, Y. S. Ko, W. D. Jang, Y. S. Jang, *Nat. Catal.* **2019**, *2*, 18–33.
- [57] A. Turner, *Environ. Sci. Technol.* **2020**, *54*, 10411–10420.
- [58] E. Jakab, M. A. Uddin, T. Bhaskar, Y. Sakata, *J. Anal. Appl. Pyrolysis* **2003**, *68–69*, 83–99.
- [59] E. Yousif, R. Haddad, *Springerplus* **2013**, *2*, 398–398.

Manuscript received: October 28, 2021
Revised manuscript received: December 15, 2021
Accepted manuscript online: December 19, 2021
Version of record online: February 23, 2022